Study of fringe effects of a two-rod capacitor embedded in a medium in order to deduce its permittivity

Xavier Chavanne, Alain Bruère, Jean-Pierre Frangi

Study of fringe Effects of a two-rod capacitor embedded in a medium in order to deduce its permittivity

Xavier Chavanne[a], Alain Bruère[b] and Jean-Pierre Frangi[a]

[a]Université de Paris, Institut de physique du globe de Paris, UMR 7154 CNRS, F-75205 Paris cedex 13, France
[b]CAPAAB, 4 Mail des Houssières, 92290 Chatenay Malabry, France;

ARTICLE HISTORY
Compiled April 15, 2020

CONTACT X. Chavanne. Orcid 0000-0002-2199-4943 Email: xavier.chavanne@univ-paris-diderot.fr

ABSTRACT
The article examines the fringe effects of a two-rod capacitor inserted in a medium like a soil due to its finite height h and presence of leads to measurement unit. The effects modify the coefficient g of conversion from probe capacitance to medium permittivity. The change of g from its expression g_{th} without effects is determined in function of probe and lead dimensions through numerical simulations and laboratory experiments. Simulations give the rise of g/g_{th} with the ratio h/D, with D the spacing of probe electrode, from about 1.09 at $h/D = 4$ to $g/g_{th} = 1.6$ at $h/D = 0.5$. Other ratio Φ/D, with Φ electrode diameter, presents a smaller influence. Experiments using different probes immersed in a liquid at different heights examine influences of leads and protective tubes around them. Contribution of leads, equivalent to a capacitor in parallel, is made negligible by keeping the ratio $\alpha_l = \Phi_l/\Phi$, where Φ_l is lead diameter, at about few percent. Choice of metallic tubes for practical reasons is not detrimental provided they are not electrically connected. Due to operating at high frequency, tubes with same voltage as the probe, in spite of acting like guards, introduce strong bias.

KEYWORDS
fringe effects; two-rod capacitor; medium permittivity; moisture sensor; dimensionless analysis; numerical and experimental studies

1. Introduction

Electric permittivity ε, and its complex conjugate the conductivity σ, of a medium such as a soil or a rock are intrinsic quantities of the medium. They can provide information like medium water content; the value of ε normalized by vacuum permittivity ε_0 ($\varepsilon_0 = 8.854$ pF·m^{-1}) - the relative permittivity ε_r - is about $\varepsilon_r = 80$ for pure water, whereas it amounts to about $\varepsilon_r = 4$ for solid constituents of soil and $\varepsilon_r = 1$ for air. Although the relation between medium bulk permittivity, permittivity of its phases and their volumetric fractions is usually not linear, these values explain the method interest. Large amount of works, from theoretical models to experiments, have been dedicated to the conversion [Hilhorst (1998)].

One of the major techniques to determine the variables ε_r and σ locally is the measurement of the capacitance - or complex admittance - of a pair of electrodes, or probe, inserted at a point in the medium [Chavanne and Frangi (2014)]. Between capacitance and permittivity exists a linear relationship of which coefficient, g, is homogeneous to a length and depends on probe shape and dimensions.

The purpose of the article is to determine the factor g in the case of a two-rod probe inserted in a medium as a function of electrode dimensions mainly. The bi-cylindrical geometry is more convenient to make and install in soils than other capacitors, such as parallel-plate capacitors. We have adopted the geometry for the soil sensors conceived and developed within our overall project called Hymenet (HYdro MEasurement NETwork) [Chavanne and Frangi (2014, 2017)]. The factor g of a two-rod probe is not easily determined except by assuming probe electric field in the medium confined between electrode ends, perpendicular to probe axis, and its amplitude constant along the axis (see [Chavanne and Frangi (2019)] for a analytical derivation of the capacitance - ε_r relationship from the electric field). Actually, this ideal situation is equivalent to have a probe infinitely long. A more realistic finite length produces a complex pattern of the electric field extending beyond electrode bases, the so-called fringe effect. As a consequence, permittivity derivation from capacitance is more complex and depends on a part of medium outside the volume around electrodes. In our knowledge, the effect for a two-rod probe has not been investigated, whereas early and abundant works have been dedicated to determine the fringe effect of

square-plate capacitors [Palmer (1937)], or disc shaped plates [Sloggett, Barton, and Spencer (1986)]. Even analytical resolutions have been carried out for both designs owing to dimensional simplifications (semi-infinite square plate, and axi-symmetry, respectively).

Moreover, additional effects modifying the factor g can arise due to practical constraints. Thus, because electrodes are inserted in the medium at a desired depth, whereas the measurement unit is placed at medium surface, a pair of leads - along protective tubes around them - are required between them. Leads act as a capacitor in parallel with the electrode one. Tubes also may introduce some electric perturbations. An alternative set-up to leads would be to connect directly the electronic unit to electrodes. However, the configuration would require to dig a trench in the medium, to assure through it power supply and data transfer, and would create stronger perturbations of medium and its inner flows. By comparison use of tubes with same geometry as electrodes - except height - reduces the perturbations. Moreover, the alternative set-up would still produce the main fringe effect, with a pattern more complex than in the case of a two-rod geometry.

Albeit different in nature, all electric effects mentioned above - called indifferently fringe effects thereafter - result in an increase of medium volume which influences probe capacitance, and in the factor g higher than its value for the ideal geometry. The work described in the article deals with all of them, together and separately, using established relationships, numerical simulations and laboratory experiments. Results are presented as the induced change on g relative to its theoretical expression g_{th} without effects, g/g_{th}. Actually measurements give the ratio of capacitances with and without effects, C/C_{th}, but both ratios coincides for a medium with uniform permittivity.

Variation is studied over the complete range of probe dimensions. It allows to weight the best compromise in face of other constraints: needs of large dimensions for good sampling volume [Chavanne and Frangi (2019)], while, on the other hand, a compact geometry is preferred to limit intrusion and to facilitate installation. Requirements of mechanical feasibility, robustness and low cost impose as well choices such as stainless steel tubes around leads. Metallic tube may influence electrode capacitance through electromagnetic interference. This choice and its consequences are equally studied in present work.

We have already carried out some numerical and experimental studies about the extent of the volume influencing probe capacitance, or sampling volume, and its dependence on probe dimensions. However, they were limited to the plane transverse to probe axis, assuming no fringe effect [Bexi, Chavanne, Conejo, and Frangi (2012); Chavanne and Frangi (2019)]. As far as the two-rod geometry is concerned, fringe effect requires a three dimension resolution of equations of the electrostatic theory, which have probably limited the work dedicated to it. Recent progress on numerical tools permits to simulate more easily fringe effects of the electric field. Simulation software are able to derive the capacitance in the case of a complex but known electrode geometry, as for instance in [Sun and Yang (2013)]. However, scope of this type of works is limited, whereas our objective is a comprehensive study of effect over a large range of probe dimensions. Moreover, perturbations introduced by leads and tubes are better investigated by laboratory experiments.

The article layout is the following: Next section gives the theoretical background on fringe effects. The set-up of both numerical and laboratory studies are then described. Finally, results are presented as plots of C change. They are discussed in view of our

objective of optimization of field sensors.

2. Materials and Methods

2.1. *Theoretical Background*

The conductance G and the capacitance C - or its admittance Y - of the probe inserted in the medium under study is related to medium apparent permittivity ε_r and conductivity σ through ($\mathbf{j}^2 = -1$):

$$Y = G + \mathbf{j}\, C\, 2\,\pi\, f = [\sigma + \mathbf{j}\, 2\pi\, f\, \varepsilon_0\, \varepsilon_r]\; g\,, \tag{1}$$

where f is the sensor frequency and g is the geometry factor with unit of length.

The quantity ε_r is the relative permittivity, which is the medium permittivity normalized by vacuum permittivity $\varepsilon_0 = 8.854$ pF·m^{-1}.

Sensor operates with alternating fields at frequency f of about 10 or more MHz in order to measure a signal related to permittivity and be able to determine medium water content. Electrostatic theory is still valid. However, inductive interaction must be included [Chavanne and Frangi (2014)].

2.1.1. Fringe Effect For a two-rod Capacitor

2.1.1.1. Generality. The factor g of a capacitor is deduced from the application of the electrostatic theory to a system made of two perfect conductors, capacitor electrodes, in total influence through a medium of permittivity ε_r. The system capacitance C, hence the factor g from Equation 1, corresponds to the charge Q on the surface of an electrode per unit of voltage $V_+ - V_-$ applied between the electrodes, $C = Q/(V_+ - V_-)$.

As the voltage is applied, an electric field $\mathbf{E}(\mathbf{r})$ is established at each point $\mathbf{r}$ of the medium. In electrostatic conditions it derives from a potential $V(\mathbf{r})$, $\mathbf{E} = \nabla V$. In general the field $\mathbf{E}$ depends on the spatial distribution of medium permittivity through Laplace's equation, $\nabla.\,[\varepsilon_r(\mathbf{r})\,\mathbf{E}(\mathbf{r})] = 0$. Assuming a uniform permittivity, as we consider in the rest of the text, the equation becomes more simply:

$$\Delta V = 0\,, \tag{2}$$

with boundary conditions of fixed potential at electrode surfaces.

The charge Q is deduced from the Gauss theorem applied at the electrodes:

$$Q = \int_S \varepsilon_0\, \varepsilon_r\, \mathbf{E}\cdot\mathbf{n}\, dS = \varepsilon_0\, \varepsilon_r \int_S \nabla\mathbf{V}\cdot\mathbf{n}\, dS\,, \tag{3}$$

where $\mathbf{n}$ is the unit vector normal to electrode surface and towards medium.

The expression of capacitance C - and hence factor g - is then:

$$C = \varepsilon_0\, \varepsilon_r\, g = \frac{\varepsilon_0\, \varepsilon_r}{(V_+ - V_-)} \int_S \nabla\mathbf{V}\cdot\mathbf{n}\, dS. \tag{4}$$

2.1.1.2. Ideal Case. In the case of two parallel cylinders of height h, diameter Φ and spacing D, the theoretical or ideal capacitance C_{th}, i.e. assuming that the electric

field is independent of h and is perpendicular to electrode axis, is (see [Chavanne and Frangi (2019)] and references therein):

$$C_{th} = \varepsilon_0 \, \varepsilon_r \, g_{th} = \frac{\varepsilon_0 \, \varepsilon_r \, h\pi}{arccosh(D/\Phi)}. \tag{5}$$

The assumption of a field direction always perpendicular to capacitor axis is less and less valid as the cylinder height h becomes smaller relative to D. A correct solution requires the treatment of equations 2 and 4 in three dimensions, as no cylindrical symmetry exists.

2.1.1.3. General Case. By working with the dimensionless potential $V^* = V/(V_+ - V_-)$ instead of the potential V, Equation 2 and its boundary conditions give the new variable as only function of space coordinates and the geometric parameters h, D and Φ. We assume that the fringe effect due to electrode finite dimensions is the only physical phenomena to consider. No other dimension has a role. As a consequence, the integral over electrode surfaces in Equation 4 - including the denominator $(V_+ - V_-)$ to make V dimensionless -, depends only on parameters h, D and Φ. We can then introduce the capacitance C_{th} of Equation 5 to make the capacitance C dimensionless, $C^* = C/C_{th}$. The latter quantity varies only with probe dimensions. Taking into account that the physical result $C^* = C/C_{th}$ should not change with the unit of length, a further simplification leads for the capacitance C to the formal expression:

$$C = C_{th} \, C^*(h/D, \alpha), \tag{6}$$

where C^* is only function of the geometric ratio h/D, as well as the ratio $\alpha = \Phi/D$ (with $\alpha < 1$ necessarily) introduced in [Chavanne and Frangi (2019)].

Actually, the dimensionless quantity $C^* = C/C_{th} = g/g_{th}$ represents the relative deviation of factor g from its expression in the ideal case given by relation 5. It tends towards one for large h/D as the assumption of field $\mathbf{E}$ perpendicular to probe axis and z-independent is more and more correct.

All results from numerical and experimental studies will be expressed in this form.

2.1.2. Lead Contribution

The pair of leads between the probe and measurement unit acts as a capacitor in parallel excited by the same voltage as applied between the electrodes. Its geometry can be approximated to the two-rod configuration of which diameter is lead diameter, Φ_l, and spacing identical to probe one, D. Each lead is protected by insulating sheath and enclosed in a tube, which separates the lead from the medium. Inner tube space is filled by air. Tubes present the same diameter Φ as the electrodes to assure a mechanical matching for better insertion and lower perturbation of medium.

Leads contribute to fringe effects if medium participates significantly to lead capacitance. In a previous study [Chavanne and Frangi (2019)] we examine how the different parts of a uniform medium around a two-rod capacitor contribute to the capacitance according to their distance from electrodes. An important parameter is the ratio of electrode diameter to their spacing. The pair of leads corresponds to a very small ratio (currently about 0.05), or to distant electrodes. In this case the distribution of medium weight to capacitance is simply modeled by Φ_l^2/r^2 at each wire with r the distance from wire center. As a consequence, contribution of medium to lead capacitance is

controlled by the ratio $\alpha_l = \Phi_l/\Phi$, which is typically $\alpha_l = 1/8$ in present prototypes. Other factors to consider are permittivity contrast between air and the medium, and the role of tube material. As for the first factor, the higher the contrast, like in the case of air/water, the weaker is medium contribution at same ratio α_l. Only experimental results will indicate exact importance of both factors.

2.1.3. Tube Effect or Diaphony

Tubes themselves may influence probe capacitance, and therefore modify g, through electromagnetic fields. It is all the more important since the medium is in contact with tubes. This effect exists only for metallic tubes and when the same voltage as between probe electrodes is imposed on them. Because tubes remain isolated from the electrodes, the layout is different from that of leads, which are a mere extension of electrodes up to the measurement unit. When electrically connected, the pair of tubes acts actually as a capacitor guard to reduce the direct fringe effect. Indeed, due to the presence of the same field at tube level, probe electric field remains perpendicular to probe axis close to electrode top, like in the ideal case.

The configuration is similar to the one used for our multi-channel sensors [Chavanne and Frangi (2014)], dedicated to measure the humidity profile in a soil. They are made of five vertically stacked capacitors, or channels, along the same cylinders, for which total height is 250 mm (each channel has a height of 50 mm), spacing 100 mm and diameter of 50 mm. Channels are successively connected to the measurement unit, while being imposed separately the same voltage between their electrodes during the whole operation. As a consequence, the direct fringe effect is confined to end capacitors acting as guards.

However, we observed some coupling between channel circuits, the so-called diaphony [Chavanne and Frangi (2014)]. We modeled and calibrated this electric effect, assuming inductive and capacitive interactions due to the use of alternating voltages at frequency f. Measurement unit provides for each capacitor k two direct voltages, $\Delta V_{Gk}^{'}$ and $\Delta V_{Ck}^{'}$, linear in first order to channel conductance and capacitance, respectively. However, those raw outputs contain a contribution from the outputs of channel m, $\Delta V_{Gm}^{'}$ and $\Delta V_{Cm}^{'}$ according to:

$$\begin{cases} \Delta V_{Gk}^{'} = \Delta V_{Gk} + \left[(ag_{km} + f_{km}\, \Delta V_{Ck}^{'})\, \Delta V_{Gm}^{'} + f_{km}\, \Delta V_{Gk}^{'}\, \Delta V_{Cm}^{'} \right] \\ \Delta V_{Ck}^{'} = \Delta V_{Ck} + \left[-f_{km}\, \Delta V_{Gk}^{'}\, \Delta V_{Gm}^{'} + (ac_{km} + f_{km}\, \Delta V_{Ck}^{'})\, \Delta V_{Cm}^{'} \right] \end{cases} \tag{7}$$

The direct voltages ΔV_{Gk} and ΔV_{Ck} in equation right-hand side represent channel k outputs without adjacent perturbations, whereas the term between brackets sums up all perturbations from channel m. Factors ag_{km}, ac_{km} and f_{km} depend on frequency f, unit sensitivity and probe geometry. We note a dependence of same phase between channels (with coefficients ag_{km} and ac_{km}), but also a cross-phase dependence such as the modification of capacitance of channel k by the conductance of channel m (coefficient f_{km}, which models inductive interaction).

In the case of our multi-channel probes, amplitudes of the parasitic effect remain below 10% of voltage values, which permits to correct the effect with reasonable uncertainty. However, the contribution may increase with channel height, or tube length. This dependence results in large errors in the case of a probe placed deep in the medium.

Like for lead, experimental study will specify these different points.

2.2. *Numerical Simulation of Main Fringe Effect*

For simplicity, numerical simulations are restricted to the study of the fringe effect without lead and tubes. Perturbations due to latter ones are better dealt with experiments, as already mentioned. Medium is also sufficiently thick below and above probe to rule out any influence of air medium interface.

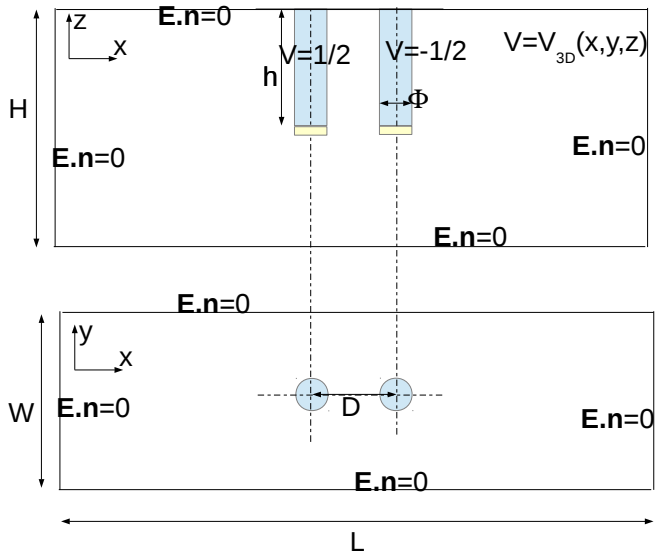

Figure 1. Front and aerial views of the domain of simulation with its dimensions and boundary conditions. The pair of electrodes are two parallel cylinders of height h, spacing D and diameter Φ. Boundary conditions at electrodes correspond to fixed potentials. L, W, H are respectively the length, the width and height of domain outer boundary. Condition at this boundary is of Neuman type.

Some commercial solvers with three-dimension capabilities are now available in line such as the one we have used, the software tools of Studio Suite from Computer Simulation Technology AG (now Dassault system Simulia Corporation). Electrostatic equations are resolved in xyz coordinates with a finite-element method over an adaptive mesh refinement. Equations 2 and 4 are thus solved in the case of a two-rod capacitor immersed in a medium of half-infinite extent at its bottom. Figure 1 shows the geometry and the dimensions of the domain of simulation, as well as the electric conditions at its boundaries. The pair of electrodes are two parallel cylinders of height h, axis distance or spacing D and diameter Φ. Boundary conditions at electrodes correspond to fixed potentials, $V_+ = +0.5$ V and $V_- = -0.5$ V. Dimensions L, W, H are respectively the length, width and depth of domain outer boundary. Condition at this boundary is of Neuman type, that is electric field must be parallel to the boundary ($\frac{\partial V}{\partial n} = 0$). As opposed to the Dirichlet type conditions (such as fixed potential), Neuman condition assures that C tends towards C_{th} at high h/D, even with the finite size of the numerical domain. Nevertheless, lateral dimensions L and W are taken some multiple of D (20 and 10 respectively), based on a previous numerical study [Bexi et al. (2012)]. The boundary choice also restricts the fringe effect at capacitor bottom, as intended for simplicity. Domain depth H is chosen sufficiently large to not impact the effect. It is fixed at 2.5 times the largest value of probe height h. To check its validity, a simulation run is performed with H six times as high as the largest h, all other parameters being unchanged. Between the two depths the change on capacitance is lower than 1% over all probe heights examined.

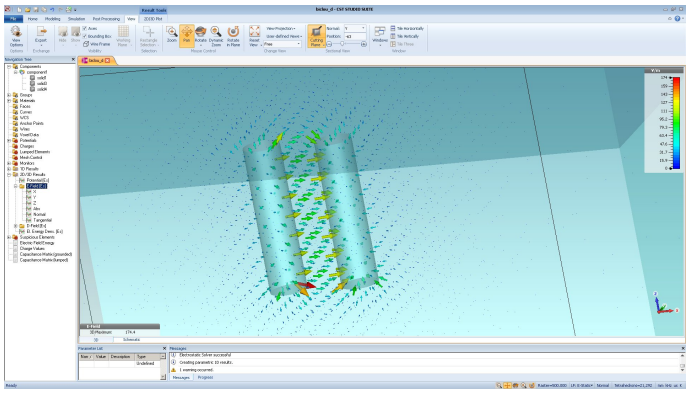

Figure 2. View of the software tools used for the numerical simulation of fringing field. The window shows the direction and intensity of the electric field of the two-rod capacitor.

The work is performed for different sets of dimensions of probe and permittivity of the medium in the domain. Dimensions in the software are formally set in mm, even if analyses are carried out with dimensionless quantities. For each fixed set of D and Φ, height h ranges from 20 to 320 mm. Electrode diameter Φ is set successively at 4, 8, 20 and 32 mm, with axis distance D unchanged at 40 mm. The case of $D = 20$ mm and $\Phi = 16$ mm is also examined to show the merit of a dimensionless analysis. For each set of dimensions, permittivity $\varepsilon_r = 2$ is varied from 10, 40, to 70, i.e. over the extreme range of values for soils.

As far as the refinement of simulation mesh is concerned, a thinner mesh around electrodes than the one used for the complete study shows equally little influence. Because the simulation was first dedicated to the study of the guards of a multi-channel sensor its end contains a thin piece of Delrin (trade name of a polymer from the Polyoxymethylene family). Due to its low permittivity ($\varepsilon_r = 2$) and thickness, its effect is negligible except for medium small permittivity (as seen in Figure 5).

The electric field deduced from the potential of Equation 2, and used to determine the capacitance, is shown in Figure 2 for one of the configuration examined.

2.3. *Experimental Set-up*

During laboratory study are recorded series of capacitance change when a liquid is progressively added over a probe completely immersed. The capacitance dependence with liquid height can be thus analyzed. Both situations, liquid in excess below electrodes and above, are examined.

The work is achieved with two recent prototypes of a same design suited to field measurement (see Figure 3 and reference [Chavanne and Frangi (2017)]). The two one-channel sensors have stainless steel electrodes of $\Phi = 8$ mm diameter and $D = 20$ mm distant (or $\alpha = 0.40$). The choice has been a compromise between a large diameter for medium sampling, availability of standardized material and sufficient space to insert a thermometer, on one side, and small footprint to limit medium perturbation, on the other size. The two sensors differ by electrode height ($h = 50$ and 70 mm), and therefore by ratio h/D. The material used for the tubes to protect the leads in the medium is also different: the short-electrode one is equipped with PMMA tubes, whereas the other one possesses stainless-steel tubes. Steel tubes are isolated from electrodes thanks to a plastic O-ring (mark (2) in photo of Figure 3). Mechanical connection between a tube and an electrode is achieved owing to a inner plastic threaded

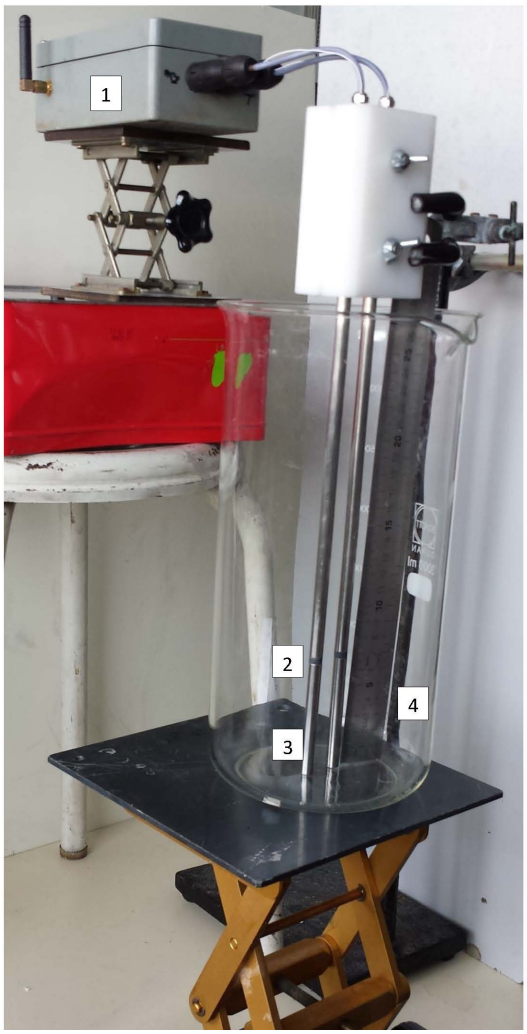

Figure 3. Experimental set-up using two similar autonomous wireless sensors. Each is composed of an electronic unit inside a housing (1), a pair of leads from unit to electrode top (2), and a pair of electrodes (3). The vertical part of leads, in the medium, is protected by a tube (made of steel in the photo). Tubes and electrodes are placed in a 13-cm inner diameter beaker progressively filled with a liquid. A metallic ruler (4) marks liquid height at each measurement. The two sensors differ by tube material - stainless steel or polymethylmethacrylate (PMMA) - and electrode height h - 70 mm or 50 mm, respectively -. For both sensors pairs of tubes and electrodes have same spacing $D = 20$ mm and diameter $\Phi = 8$ mm.

pin screwed into them. The difference of tube material between sensors permits to measure their contribution to the fringe effect. Tubes and electrodes have the same diameter essentially to facilitate insertion and reduce perturbations to medium. During laboratory study a plastic block made of two bridge-shaped parts maintains the two tubes and electrodes parallel at spacing $D = 20$ mm.

Sensors have been calibrated as admittance-meter, according to the procedure described in [Chavanne and Frangi (2017)]. Various liquids of known permittivity and conductivity, from hexanol_1 to water with dissolved KCl salt, are used to carry it out. Liquids cover just the probe. Due to permittivity contrast between a liquid and air, or baker glass, we assume that electric field is ideally parallel to the interference and remains perpendicular to electrodes like in the ideal case. As a result, capacitance and conductance are deduced from permittivity and conductivity, respectively, using

Equation 5. Afterwards, sensor outputs give the capacitance and conductance to any situation.

Liquids used for the present study are two alcohols - methanol and propanol_1 - and water. The alcohols present permittivity close to a mildly wet soil (ε_r are respectively 32.7 and 20.1 at 25°C). Influence of salinity is also examined with solutions of water, or methanol, and KCl (with a conductivity of around 500 μS·cm^{-1}). Methanol is one of the few alcohols to dissolve significant KCl quantity.

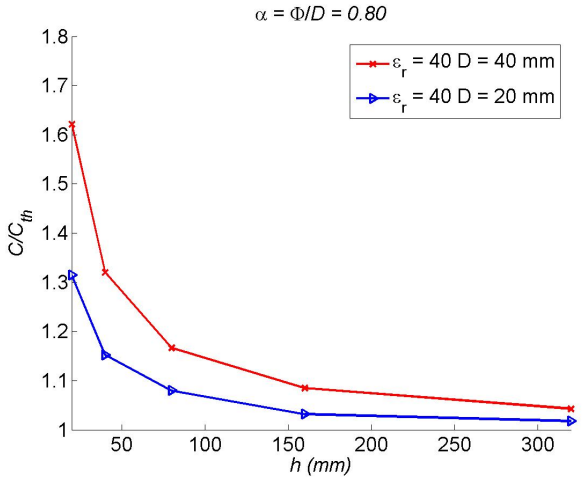

(a)

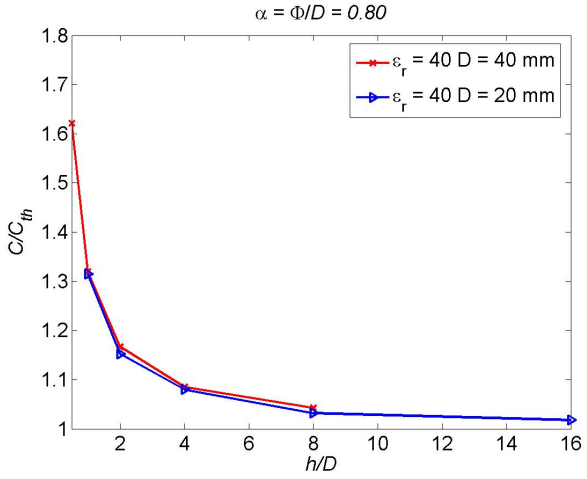

(b)

Figure 4. Deviation from the theoretical capacitance, C/C_{th}, as a function of electrode height h obtained from numerical simulations for two different electrode spacings D. In graph (**a**) C/C_{th} is plotted against h. In graph (**b**) it is plotted against ratio h/D. Matching curves in graph (**b**) shows the pertinence of a dimensionless analysis. Ratio $\alpha = \Phi/D$, with Φ electrode diameter, and medium permittivity ε_r are maintained constant.

Electrodes are placed in a 13-cm inner diameter beaker (see Figure 3). The recipient is filled with a liquid step by step from a reference state in which only electrodes are immersed. At each step capacitance is measured by the sensor while a metallic ruler marks liquid height. Hence, is measured a series of capacitances, C, and corresponding heights of liquid in excess from electrode ends, Δh. The capacitance at the first step, $\Delta h = 0$, constitutes the reference capacitance C_{ref}, from which is calculated the dimensionless quantity C/C_{ref}. Because of permittivity contrast, as mentioned,

C_{ref} and the ideal capacitance C_{th} from Equation 5 are confounded. As a result, the deviation g/g_{th} from the ideal geometry is recorded in function of Δh made dimensionless with h. The procedure also permits to reduce measurement uncertainty by offsetting common errors. Measurements performed with liquid below the electrodes are achieved using a laboratory jack to lower the beaker with the liquid. The quantity Δh is counted negatively. This set-up produces only the pure fringe effect (paragraph 2.1.1), as tubes are not covered. For liquid above electrodes all effects are present.

Uncertainty on height from measurement with the ruler amounts to $\delta\Delta h = \pm 0.5$ mm. Uncertainty on capacitance measurement arises from difficulty to appreciate the coincidence of liquid level with electrode top due to capillary effect and parallax error. With minimization of the latter one, uncertainty on $\delta C/C$ and $\delta C_{ref}/C_{ref}$ is assessed at about $\pm 1\%$. Using error propagation, we deduce the uncertainty on dimensionless capacitance $C^* = C/C_{th}$ from measurement errors:

$$\delta C^{*\,2} \simeq (C/C_{ref})^2 \left[(\delta C/C)^2 + (\delta C_{ref}/C_{ref})^2 \right],$$

or, taking into account that $C^* = C/C_{th}$ remains close to 1:

$$\delta C^* \sim \pm\,(C/C_{th})\ 0.015 \sim \pm 0.015. \tag{8}$$

3. Results and Discussion

3.1. *Simulation Study*

Figure 4 demonstrates the pertinence of a dimensionless analysis using Equation 6. Two series of dimensionless capacitances C/C_{th} obtained for various electrode heights h each with a different spacing - $D = 20$ and 40 mm -, match each other if plotted versus h/D and not h. The other dimensionless geometric parameter, $\alpha = \Phi/D$, and permittivity are maintained constant (at $\alpha = 0.80$ and $\varepsilon_r = 40$). Below $h/D = 4$ the quantity C/C_{th} rises rapidly from about $C/C_{th} = 1.1$ to $C/C_{th} = 1.6$ at $h/D = 0.5$.

Figure 5 shows the influence of permittivity on the curves C/C_{th} versus h/D. Theoretically no effect should be detectable. However, the curve obtained at permittivity $\varepsilon_r = 2$ presents larger values than others at higher permittivity. The discrepancy may result from the presence of the thin piece of plastic at electrode end by construction. In the case of a one-channel sensor the piece is absent and, therefore, probably the effect too.

Figure 6 presents the dependence of the plots C/C_{th} versus h/D on the other dimensionless geometric parameter, $\alpha = \Phi/D$. Between $\alpha = 0.1$ - distant electrodes - and $\alpha = 0.5$ - close electrodes - the capacitance C/C_{th} increases with α at constant h/D. For $h/D = 3.5$ the quantity C/C_{th} varies from 1.075 to 1.13. The effect is a little reversed at higher α. Raising electrode diameter, all other dimensions being equal, enhances the extent of electric field around the probe. This observation is consistent with the conclusion in ref. [Chavanne and Frangi (2019)] that a large diameter increases the sampling volume of medium.

The two dashed lines in Figure 6 indicate the respective height, $h/D = 2.5$ and 3.5, of the two sensors used in the laboratory study (for which $\alpha = 0.4$). According to numerical simulations, capacitance for the two sensors rises respectively by about 10% and 15% relative to the ideal one of Equation 5.

In the case of a multi-channel sensor, of which ratio h/D is 2.5 - probe overall height

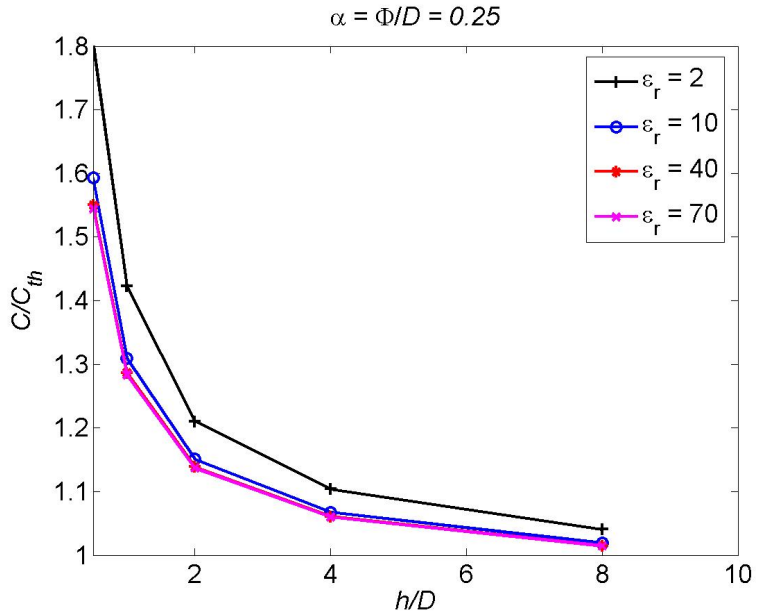

Figure 5. Influence of medium permittivity ε_r on plots C/C_{th} versus ratio h/D according to numerical simulations. The ratio $\alpha = \Phi/D$ is fixed. See Figure 4 and text for notations.

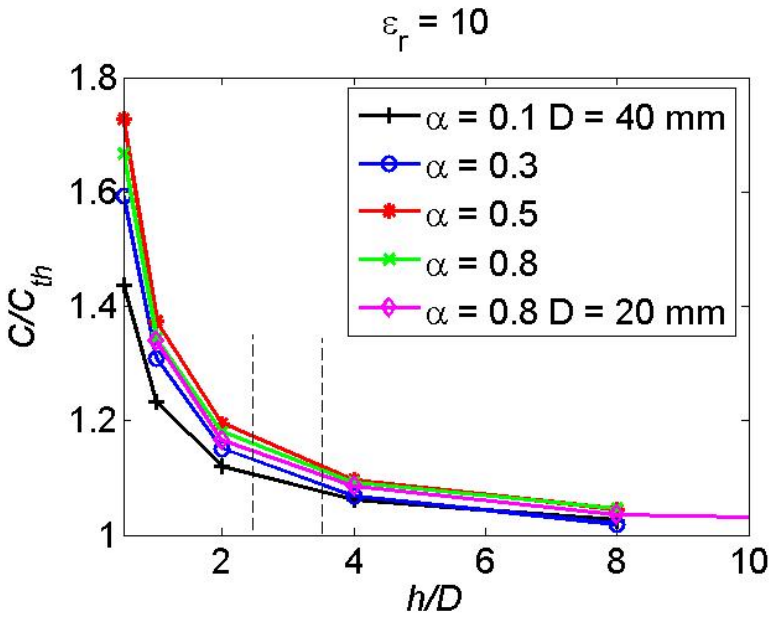

Figure 6. Dependence of the plots C/C_{th} versus h/D on the ratio $\alpha = \Phi/D$ at same medium permittivity, according to numerical simulations. The two dashed lines show the values of h/D for the two sensors used in the laboratory study. The other geometric ratio is $\alpha = 0.4$. See Figure 4 for notations.

must be considered - and the other is $\alpha = 0.5$, the value of C/C_{th} reaches 1.15, i.e. a capacitance higher than C_{th} by more than 15%. However, this factor applies only to each end channel acting as guard. In new multi-channel prototypes for which electrode diameter is 30 mm and height the same as for previous sensors, the spacing can be lessened to $D = 70$ mm to diminish the effect.

3.2. *Experimental Study*

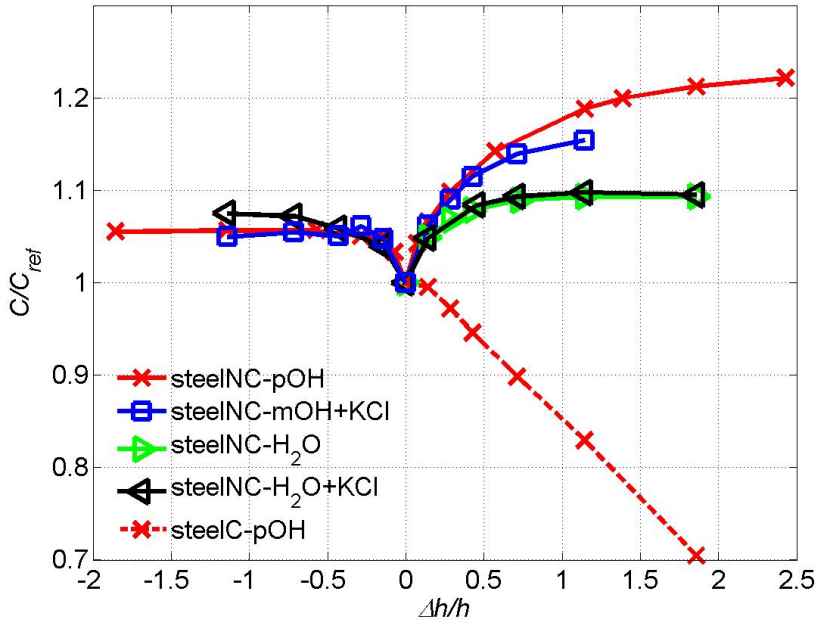

Figure 7. Variation of the dimensionless capacitance C/C_{th} with excess liquid height $\Delta h/h$ below ($\Delta h/h < 0$) and above electrodes ($\Delta h/h > 0$), according to experiments. C_{th} is the theoretical capacitance (Equation 5). Sensor is equipped with stainless steel tubes to protect leads above electrodes. h is electrode height. Tubes are either connected (C) to maintain the same potential as their respective electrode, or performed without connection (NC). Different liquids are tested in the latter setup (mOH: methanol, pOH: propanol_1 and H_2O: water. +KCl: salt KCl added.

In the case of the sensor equipped with steel tubes Figure 7 shows the difference of behaviors between tubes electrically connected and not. In the first configuration each tube is maintained at the same potential as the electrode it is screwed to. As a consequence, departure from the ideal capacitance C_{ref} increases linearly with the thickness Δh of liquid layer above electrodes. This observation is consistent with the diaphony phenomenon as described in paragraph 2.1.3. In the configuration without connection the capacitance appears to level off with excess height. Therefore, the choice looks better, in spite that the other setup should act as a guard to fringe effect. Following experiments are performed with non-connected tubes.

Figure 8 shows variations of the ratio C/C_{ref} with excess liquid height $\Delta h/h$ below ($\Delta h/h < 0$) and above electrodes ($\Delta h/h > 0$) for both sensors and various liquids. Whatever the situation the quantity C/C_{ref} appears to level off with excess height Δh, in general beyond a value of Δh between half and one h.

In the case of liquid only in excess below electrodes, or $\Delta h/h < 0$, the difference of asymptotic capacitance between the two sensors is consistent with results of the numerical study, for which only the direct fringe effect is present: large ration h/D gives asymptotic C/C_{ref} closer to one, that is the ideal case. However, the asymptotic values depend, albeit slightly, on the liquid permittivity. They are largest for water, with the highest permittivity. They present a better agreement with numerical results ($C/C_{ref} = 1.08$ and 1.14 for $h = 70$ mm and $h = 50$ mm, respectively). A plausible explanation is the existence of a residual fringe effect in the reference case - $\Delta h/h = 0$ - all the larger as liquid permittivity is closer to that of air and, therefore, permittivity

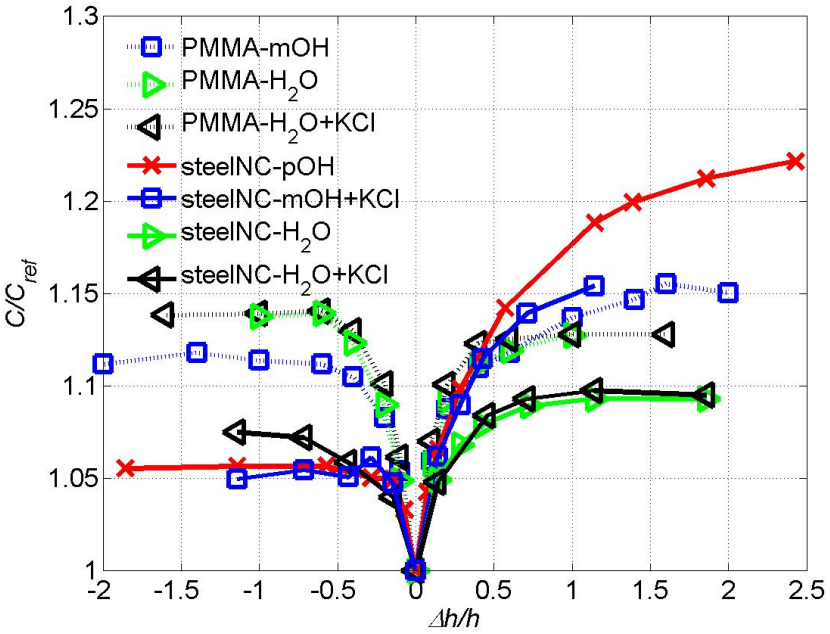

Figure 8. Dimensionless capacitance C/C_{ref} in function of excess liquid height $\Delta h/h$ below ($\Delta h/h < 0$) and above electrodes ($\Delta h/h > 0$), from experiments. See Figure 7 for notations. Tubes above electrodes are made of either stainless steel or polymethyl methacrylate - PMMA -. Electrode heights are $h = 70$ mm in the case of steel, while $h = 50$ mm for plastic. Both have same diameter and spacing.

contrast is smaller.

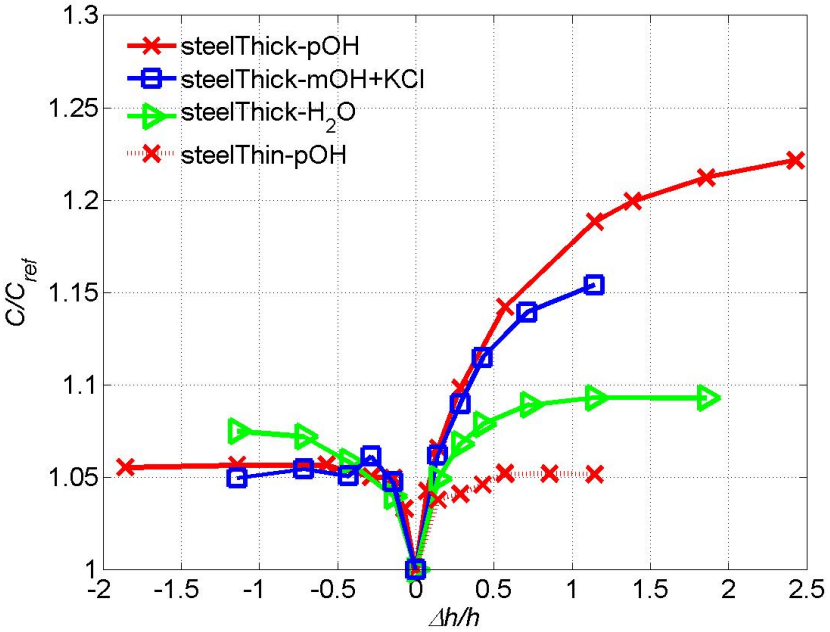

Figure 9. Same as Figure 8 limited to data from sensor with unconnected stainless-steel tubes. The additional curve C/C_{ref} versus $\Delta h/h$ for $\Delta h/h > 0$ using propanol_1 - *steelThin-pOH* - corresponds to lead four times as thin as lead in the previous sensor setup.

In the case of liquid in excess above electrodes, or $\Delta h/h > 0$, measurements should be affected by all the fringe effects, as described in part 2.1. Indeed, in general asymptotic values of C/C_{ref} are higher in the right-hand side of Figure 8, liquid above electrodes, than in the left-hand side, liquid below electrodes. However, the difference depends on tube material and liquid. It is more pronounced for alcohols than for water, and/or for steel tubes than plastic, being negligible in the case of water and plastic. A good explanation is the contribution to C of the pair of leads inside the tubes acting as a capacitor. Probably, a metallic tube and a permittivity contrast between medium and air insufficiently large compound the effect. From paragraph 2.1.2, the main parameter controlling it is the ratio $\alpha_l = \Phi_l/\Phi$, where Φ_l is lead diameter and Φ tube diameter. Leads of current sensors present a diameter of about $\Phi_l = 1$ mm with $\Phi = 8$ mm, or $\alpha_l = 0.125$. For alcohols, to which soil permittivity is close, the effect is not negligible. Therefore the quantity α_l must be reduced further.

In a recent sensor leads have been swapped for thinner ones, of which diameter is $\Phi_l = 0.25$ mm. As a consequence, the ratio $\alpha_l = \Phi_l/\Phi$ is four times as low as in current sensors, and fringe effects are dramatically reduced as seen in Figure 9. An adverse effect would be an increase of lead resistance. However, the resistance remains lower than 1 Ω (the rise is limited due to the importance of skin effect at $f = 24$ MHz), which is acceptable.

Table 1. Heights of liquid in excess above, $\Delta h_h/h$, and below, $\Delta h_b/h$, electrodes and associated dimensionless capacitance C/C_{ref}. Measurement achieved in propanol_1 with $h = 70$ mm-height electrodes and steel tubes.

$\Delta h_h/h$	$\Delta h_b/h$	C/C_{ref}
0.14	0.00	1.06+/-0.01
0.00	-0.14	1.05+/-0.01
0.14	-0.14	1.12+/-0.01
0.29	0.00	1.09+/-0.01
0.00	-0.43	1.08+/-0.01
0.29	-0.43	1.17+/-0.01
0.43	0.00	1.12+/-0.01
0.00	-0.71	1.08+/-0.01
0.43	-0.71	1.20+/-0.01
0.71	0.00	1.16+/-0.01
0.00	-1.14	1.08+/-0.01
0.71	-1.14	1.24+/-0.01

Some measurements are performed with liquid both below and above electrodes to study how to take into account this more common situation by comparison with liquid present only either above or below. Table 1 shows that corrections on capacitance are approximately additive, which makes the overall correction larger but easier to deal with.

3.3. *Application to a New Sensor*

Taking into account results and conclusion obtained through the article, as well as constraints previously identified such as a representative sampling volume and use of steel tubes, we can design the probe and lead of a one-channel sensor and determine the correction to include in g_{th} to deduce medium permittivity. Electrode dimensions are fixed at a height $h = 70$ mm, diameter $\Phi = 8$ mm and axis distance $D = 20$ mm, or ratios $h/D = 3.5$ and $\alpha = 0.40$. Leads to measurement unit have a diameter

$\Phi_l = 0.25$ mm, or a ratio $\alpha_l = \Phi_l/\Phi = 1/32$. Steel tubes to protect leads have same diameter and spacing as electrodes.

From this configuration, for a probe sufficiently buried in soil (about about distance h from surface), we expect a corrective factor g/g_{th} of two times $1.09 = 1.18$ from Figures 6 and 9.

4. Conclusions

The article have studied the fringe effects of a two-rod capacitor inserted in a medium, due to its finite height, and due to medium electrical influence on leads between capacitor and measurement circuit at medium surface. Practical considerations and measurements constraints impose leads and a protective tube around each of them. Fringe effects affect the conversion from probe capacitance to medium local permittivity, hence the determination of its water content deduced from permittivity. The coefficient of conversion, the geometric factor g, increases with the effects from its theoretical expression without them, g_{th}.

Effects have been examined through numerical simulations and laboratory experiments in relation with established relationships. The work have permitted to discriminate between the different effects and to determine quantitatively the dependences of the factor change, g/g_{th}, which is also the capacitance change, C/C_{th}. Simulations, limited to the effect due to probe finite height, have established the variation with geometric ratio h/D, where h is probe height and D spacing of probe electrodes. The quantity g/g_{th} rises rapidly from about $C/C_{th} = 1.08$ at $h/D = 4$ to $C/C_{th} = 1.6$ at $h/D = 0.5$. Other ratio Φ/D, where Φ is electrode diameter, has a lower influence.

Laboratory experiments consist on two probes with different h and material of tubes - plastic or metal -immersed in a liquid - alcohols or water - at different heights. Results agree with simulation outputs and extend the study to effects due to leads and tubes. Metallic tubes, in spite of being more robust and cheaper, may interfere with probe measurement resulting in an increase of g/g_{th}. Importantly, if the same voltage as the probe is imposed to tubes, the effect is overwhelming, in spite of tubes acting like guards against the direct fringe effect. The best setup is no electric connection.

Leads contribute to fringe effects if medium participates significantly to lead capacitance. The influence is controlled by another geometric ratio, $\alpha_l = \Phi_l/\Phi$, where Φ_l is lead diameter and Φ tube diameter, identical to electrode one by design. Space between lead and tube is filled by plastic of sheath and air, that is with no effect on fringe effect. However, current design with ratio $\alpha_l = 1/8$ does not prevent medium influence. By using thinner leads - ratio $\alpha_l = 1/32$ - effects due to leads and tubes have almost disappeared. For a prototype with these characteristics and with probe ratio h/D at 3.5, correction on g_{th} amounts to about 1.18.

We can thus determine accurately the water content of a medium via permittivity at any depths thanks to a cost-effective and robust sensor, which equally introduces low perturbations to the medium and its flows.

Disclosure statement

The authors declare no conflict of interest.

References

Bexi, I., Chavanne, X., Conejo, E., & Frangi, J.-P. (2012). Validation of a complex permittivity meter for porous media operating between 1 and 20 mhz. *Instrumentation and Measurement, IEEE Transactions on*, *61*(7), 2000–2011.

Chavanne, X., & Frangi, J.-P. (2014). Presentation of a complex permittivity-meter with applications for sensing the moisture and salinity of a porous media. *Sensors*, *14*(9), 15815–15835.

Chavanne, X., & Frangi, J.-P. (2017). Autonomous sensors for measuring continuously the moisture and salinity of a porous medium. *Sensors*, *17*(5), 1094.

Chavanne, X., & Frangi, J.-P. (2019). Sample volume of a capacitance moisture sensor in function of its geometry. *European Journal of Environmental and Civil Engineering*, *0*(0), 1-19. Retrieved from `https://doi.org/10.1080/19648189.2018.1500311`

Hilhorst, M. (1998). *Dielectric characterisation of soil* (Unpublished doctoral dissertation). Agricultural University of Wageningen, Wageningen, The Netherlands.

Palmer, H. B. (1937). The capacitance of a parallel-plate capacitor by the schwartz-christoffel transformation. *Electrical Engineering*, *56*(3), 363–368.

Sloggett, G., Barton, N., & Spencer, S. (1986). Fringing fields in disc capacitors. *Journal of Physics A: Mathematical and General*, *19*(14), 2725.

Sun, J., & Yang, W. (2013). Fringe effect of electrical capacitance and resistance tomography sensors. *Measurement science and technology*, *24*(7), 074002.